

Detection of bridge emission above 50 GeV from the Crab pulsar with the MAGIC telescopes

J. Aleksić¹, S. Ansoldi², L. A. Antonelli³, P. Antoranz⁴, A. Babic⁵, P. Bangale⁶, U. Barres de Almeida⁶, J. A. Barrio⁷, J. Becerra González^{8,26}, W. Bednarek⁹, E. Bernardini¹⁰, B. Biasuzzi², A. Biland¹¹, O. Blanch¹, S. Bonnefoy⁷, *, G. Bonnoli³, F. Borracci⁶, T. Bretz^{12,27}, E. Carmona¹³, A. Carosi³, P. Colin⁶, E. Colombo⁸, J. L. Contreras⁷, J. Cortina¹, S. Covino³, P. Da Vela⁴, F. Dazzi⁶, A. De Angelis², G. De Caneva¹⁰, B. De Lotto², C. Delgado Mendez¹³, M. Doert¹⁴, D. Dominis Prester⁵, D. Dorner¹², M. Doro¹⁵, S. Einecke¹⁴, D. Eisenacher¹², D. Elsaesser¹², E. Farina¹⁶, D. Ferenc⁵, D. Fidalgo⁷, M. V. Fonseca⁷, L. Font¹⁷, K. Frantzen¹⁴, C. Fruck⁶, R. J. García López⁸, M. Garczarczyk¹⁰, D. Garrido Terrats¹⁷, M. Gaug¹⁷, N. Godinović⁵, A. González Muñoz¹, S. R. Gozzini¹⁰, D. Hadasch¹⁸, M. Hayashida¹⁹, J. Herrera⁸, A. Herrero⁸, D. Hildebrand¹¹, K. Hirotani²⁰, *, J. Hose⁶, D. Hrupec⁵, W. Idec⁹, V. Kadenius²¹, H. Kellermann⁶, K. Kodani¹⁹, Y. Konno¹⁹, J. Krause⁶, H. Kubo¹⁹, J. Kushida¹⁹, A. La Barbera³, D. Lelas⁵, N. Lewandowska¹², E. Lindfors^{21,28}, S. Lombardi³, M. López⁷, R. López-Coto¹, A. López-Oramas¹, E. Lorenz⁶, I. Lozano⁷, M. Makariev²², K. Mallot¹⁰, G. Maneva²², N. Mankuzhiyil², K. Mannheim¹², L. Maraschi³, B. Marcote²³, M. Mariotti¹⁵, M. Martínez¹, D. Mazin⁶, U. Menzel⁶, J. M. Miranda⁴, R. Mirzoyan⁶, A. Moralejo¹, P. Munar-Adrover²³, D. Nakajima¹⁹, A. Niedzwiecki⁹, K. Nilsson^{21,28}, K. Nishijima¹⁹, K. Noda⁶, N. Nowak⁶, R. Orito¹⁹, A. Overkemping¹⁴, S. Paiano¹⁵, M. Palatiello², D. Paneque⁶, R. Paoletti⁴, J. M. Paredes²³, X. Paredes-Fortuny²³, S. Partini⁴, M. Persic^{2,29}, P. G. Prada Moroni²⁴, E. Prandini¹¹, S. Preziuso⁴, I. Puljak⁵, R. Reinthal²¹, W. Rhode¹⁴, M. Ribó²³, J. Rico¹, J. Rodriguez Garcia⁶, S. Rügamer¹², A. Saggion¹⁵, T.Y. Saito¹⁹, *, K. Saito¹⁹, K. Satalecka⁷, V. Scalzotto¹⁵, V. Scapin⁷, C. Schultz¹⁵, T. Schweizer⁶, S. N. Shore²⁴, A. Sillanpää²¹, J. Sitarek¹, I. Snidaric⁵, D. Sobczynska⁹, F. Spanier¹², V. Stamatescu¹, A. Stamerra³, T. Steinbring¹², J. Storz¹², M. Strzys⁶, S. Sun⁶, T. Surić⁵, L. Takalo²¹, H. Takami¹⁹, F. Tavecchio³, P. Temnikov²², T. Terzić⁵, D. Tesaro⁸, M. Teshima⁶, J. Thaele¹⁴, O. Tibolla¹², D. F. Torres²⁵, T. Toyama⁶, A. Treves¹⁶, M. Uellenbeck¹⁴, P. Vogler¹¹, R. M. Wagner^{6,30}, and R. Zanin²³, *

(Affiliations can be found after the references)

Submitted 18 February 2014, Accepted 24 April 2014

ABSTRACT

Context. The Crab pulsar is the only astronomical pulsed source detected at very high energy (VHE, $E > 100$ GeV) gamma rays. The emission mechanism of VHE pulsation is not yet fully understood, although several theoretical models have been proposed.

Aims. In order to test new models, we measured the light curve and the spectra of the Crab pulsar with high precision by means of deep observations.

Methods. We analyzed 135 hours of selected MAGIC data taken between 2009 and 2013 in stereoscopic mode. In order to discuss the spectral shape in connection with lower energies, 5.5 years of *Fermi*-LAT data were also analyzed.

Results. The known two pulses per period were detected with a significance of 8.0σ and 12.6σ . In addition, significant emission was found between the two pulses with 6.2σ .

Conclusions. We discovered the bridge emission above 50 GeV between the two main pulses. This emission can not be explained with the existing theories. These data can be used for testing new theoretical models.

Key words. pulsars: individual: Crab pulsar – gamma rays: stars

1. Introduction

The Crab pulsar and the surrounding Crab nebula are the remnant of the supernova of AD 1054. It is one of the youngest pulsars known and its spin down luminosity (4.6×10^{38} erg/s) is the highest among Galactic neutron stars. A remarkable feature of

the Crab pulsar is that it is visible at all wavelengths, from radio (10^{-5} eV) to VHE gamma rays ($> 10^{11}$ eV). To date, this pulsar is the only one for which pulsed emission has been detected above 100 GeV.

Gamma-ray pulsation from the Crab pulsar up to ~ 10 GeV had been known since the 1990s from EGRET observations (Nolan et al. 1993). In 2008, pulsations were found by the MAGIC telescope at energies above 25 GeV (Aliu et al. 2008). This result suggested that the emission originates in the outer magnetosphere. The simplest curvature radiation scenario in

* Corresponding authors: T. Y. Saito e-mail: tysaito@cr.scphys.kyoto-u.ac.jp, R. Zanin e-mail: rzanin@am.ub.es, S. Bonnefoy e-mail: simon@gae.ucm.es and K. Hirotani e-mail: hirotani@tiara.sinica.edu.tw

the outer magnetosphere predicts an exponential cutoff in the energy spectrum at GeV energies (e.g., Muslimov & Harding 2004; Takata et al. 2006; Tang et al. 2008). *Fermi*-LAT observations from 100 MeV to a few tens of GeV, which started in August 2008, showed a clear break in the spectrum at ~ 6 GeV (Abdo et al. 2010) supporting this scenario. A few years later, however, MAGIC and VERITAS (Aleksić et al. 2011, 2012a; Aliu et al. 2011) found that the energy spectrum of the Crab pulsar extends up to 400 GeV following a power law. The emission above 100 GeV is difficult to explain only with the curvature radiation, and additional or different emission mechanisms are required. Several new models were recently proposed to explain the energy spectrum of the Crab pulsar (e.g., Aleksić et al. 2011; Aharonian et al. 2012).

Here we present new results from the continuing monitoring of the Crab pulsar with the MAGIC telescopes that will help to constrain any model for the emission. In order to discuss the Crab pulsar spectra at energies lower than those accessible to MAGIC, *Fermi*-LAT data were also analyzed.

2. Instruments, data sets, and analysis methods

2.1. The MAGIC Telescopes

The MAGIC telescopes are two Imaging Atmospheric Cherenkov Telescopes located on the island of La Palma (Spain) at 2200 m above sea level. Both telescopes consist of a 17 m diameter reflector and a fast imaging camera with a field of view of 3.5° . The trigger threshold for regular observations at zenith angles below 35° is around 50 GeV and the sensitivity above 290 GeV (in 50 h) is 0.8% of the Crab nebula flux with an angular resolution better than 0.07° (Aleksić et al. 2012b). The first telescope started operation in 2004, while the second one became operational in 2009.

For this study we used 135 hours of data taken at zenith angles below 35° during optimal technical and weather conditions between September 2009 and April 2013. Standard MAGIC analysis, as described in Moralejo et al. (2009) and Aleksić et al. (2012b), was applied to the data. The conversion from event arrival times to pulsar rotational phases used *Tempo2* software (Hobbs et al. 2006) and a dedicated package inside MARS (López 2006). The spin parameters of the Crab pulsar were taken from the monthly reports of the Jodrell Bank Radio telescope¹ (Lyne et al. 1993).

2.2. Fermi-LAT

The Large Area Telescope (LAT) is a pair conversion gamma-ray detector on board the *Fermi* satellite (Atwood et al. 2009). It can detect high-energy gamma rays from 20 MeV to more than 300 GeV. It has been operational since August 2008 and all the collected data are publicly available. In this work, we have used 5.5 years of Pass 7 reprocessed data² from 2008 August 4 to 2014 January 31. The region of interest was chosen to be 30° around the Crab pulsar.

Along with the public data, the LAT team provides the corresponding analysis software and instrument response functions (IRF) designed for the analysis of that particular dataset. We have used the version v9r32p5 of the *Fermi*-LAT ScienceTools³

and the P7REP_SOURCE_V15 IRF. From the downloaded data we have discarded events taken at zenith angles above 100° to reduce the contamination of albedo gamma rays coming from the Earth's limb. To compute the pulse phase, we used the same spin parameters as for the MAGIC analysis. The obtained fluxes were computed by maximizing the likelihood of a given source model using the *gtlike* tools. The binned likelihood method was adopted and a 40° square area with 0.2° bin width was used for the likelihood maximization. Apart from the Galactic (*gal_lem_v05.fits*) and extragalactic (*iso_source_v05.txt*) diffuse emission, we considered as background sources for the likelihood fits all sources listed in the second LAT source catalogue (Nolan et al. 2012). The data taken during the periods when the Crab nebula was flaring were not excluded from the analysis. These flares should not have any impact on the pulsed emission results because it is known that the pulsation component did not change during the flares (Buehler et al. 2012), and the average nebula flux including flare periods was subtracted when the pulsar signal was determined. Regarding the reported *Fermi*-LAT spectrum from the Crab nebula, the six Crab flares that lasted a few days might be responsible for a few percent of the photons below 1 GeV in the overall 5.5 year dataset. Given that the effect is expected to be small, and that this paper focusses on the emission from the pulsar, we did not correct for this effect.

3. Results

3.1. Light curve above 50 GeV

Figure 1 shows the light curves of the Crab pulsar measured by MAGIC. Two peaks are clearly visible. Following our previous study (Aleksić et al. 2012a), we define phase ranges for the two peaks as $P1_M$ (phase -0.017 to 0.026) and $P2_M$ (0.377 to 0.422). The background level (hadrons and continuum gamma rays) is estimated using the phase range between 0.52 and 0.87 and it is then subtracted from the histograms⁴. The number of excess events in $P1_M$ between 50 GeV and 400 GeV is 930 ± 120 (8.0σ) and in $P2_M$ is 1510 ± 120 (12.6σ).

In addition to the two main peaks, significant emission between them is also visible. The region between the peaks is generally called the Bridge. Defining the Bridge region as the gap between $P1_M$ and $P2_M$, namely, between 0.026 and 0.377 (hereafter $Bridge_M$), we obtain an excess of 2720 ± 440 (6.2σ) events in this region. Adopting the definition used at lower energies for the Bridge as the region $0.14 - 0.25$ from Fierro et al. (1998) (hereafter $Bridge_E$), then the number of excess events is 880 ± 200 (4.4σ). This excess increases to 1940 ± 370 (5.2σ) if we extend $Bridge_E$ with the so-called trailing wing of P1 and the leading wing of P2, namely to the interval of $0.04 - 0.32$ (see Fierro et al. 1998). It should be noted that this detection confirms the hint of bridge emission already reported in (Aleksić et al. 2012a).

3.2. Comparison with lower energies

Figure 2 shows the light curves at optical, X-ray, and gamma-ray energies obtained with various instruments, together with the 50 – 400 GeV light curve from the bottom panel of Fig. 1. The background was subtracted in the same way as the MAGIC light curves (see Sect. 3.1). The intensity and morphology of the

⁴ An estimation of the background using the off-peak interval from the LAT Second Pulsar Catalog, namely the phase range between 0.61 and 0.89 , lead to very similar results.

¹ <http://www.jb.man.ac.uk/~pulsar/crab.html>

² http://fermi.gsfc.nasa.gov/ssc/data/analysis/documentation/Pass7REP_usage.html

³ <http://fermi.gsfc.nasa.gov/ssc/data/analysis/scitools/overview.html>

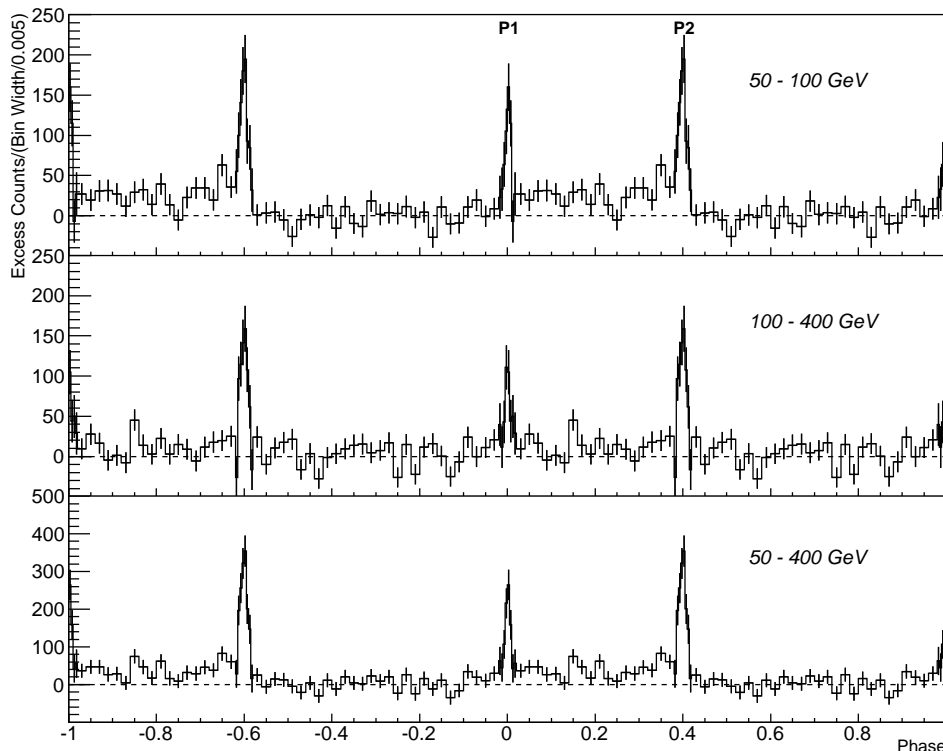


Fig. 1. Light curves of the Crab pulsar obtained by MAGIC from 50 GeV to 100 GeV (top), from 100 GeV to 400 GeV (middle), and for the full analyzed energy range (bottom). The bin widths around the peaks are 4 times smaller (0.005) than the rest (0.02) in order to highlight the sharpness of the peaks.

bridge emission varies considerably with energy. It is very weak at optical wavelengths and in the 100 – 300 MeV range, while there is an appreciable difference at X-rays and soft gamma rays. At the energies covered by MAGIC, the peaks get much sharper and a prominent bridge emission appears.

It is known that the flux ratio between the two peaks strongly depends on energy, as does the ratio between the first peak and the bridge (see, e.g., Kuiper et al. 2001). Fig. 3 shows the flux ratio between $P2_M$ and $P1_M$ and that between $Bridge_E$ and $P1_M$ as a function of energy from optical (~ 2 eV) to 400 GeV. Steady emission was subtracted before the ratios were computed. The ratios $P2_M/P1_M$ and $Bridge_E/P1_M$ behave similarly. These ratios increase with energy up to 1 MeV, decrease up to 100 MeV, and increase again from that energy on. At 50 – 400 GeV, the ratios basically follow the trend seen at lower energies.

3.3. Spectral energy distribution

The spectral energy distributions (SEDs) of the $P1_M$, $P2_M$, $Bridge_M$, and $Bridge_E$ between 100 MeV and 400 GeV are shown in Fig. 4, together with the Crab nebula SED obtained with a subset of the data used for the pulsar analysis. The SEDs were calculated using *Fermi*-LAT data below 50 GeV (below 200 GeV for the nebula), and MAGIC data above 50 GeV. The nebula SED is connected smoothly between the two instruments. The *Fermi*-LAT data were fit with a power law with an exponential cutoff, while the MAGIC data were fit with a simple power-law function. The obtained fit parameters are summarized in Table 1. The power-law indices between 50 GeV and 400 GeV are about 3 and no significant difference is seen between different pulse phases. The uncertainty in the absolute energy scale is

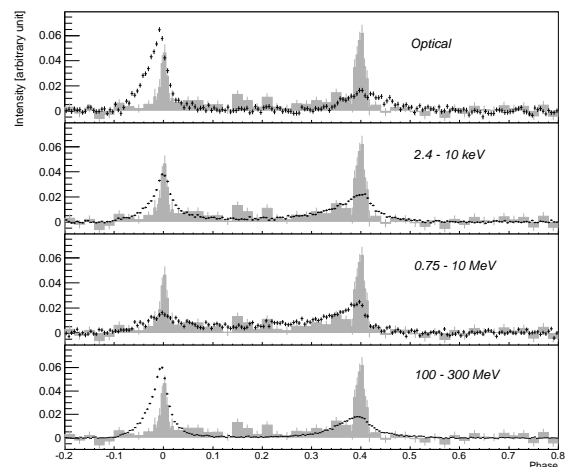


Fig. 2. Light curve of the Crab pulsar at optical wavelength, 2.4 – 10 keV X-rays, 0.75 – 10 MeV, and 100 – 300 MeV gamma rays (from top to bottom). The light curve at 50 – 400 GeV is overlaid on each plot for comparison. The optical light curve was obtained with the MAGIC telescope using the central pixel of the camera (Lucarelli et al. 2008). The keV and MeV light curves are from Kuiper et al. (2001). The 100 – 300 MeV light curve was produced using the *Fermi*-LAT data. All light curves are zero-suppressed by estimating the background using the events in the phase range from 0.52 to 0.87.

estimated as 17%, whereas the systematic error of the flux normalization is estimated to be 18%. The difference between this number and the one given in Aleksić et al. (2012b) is mainly due to a more precise background estimation from the off-peak re-

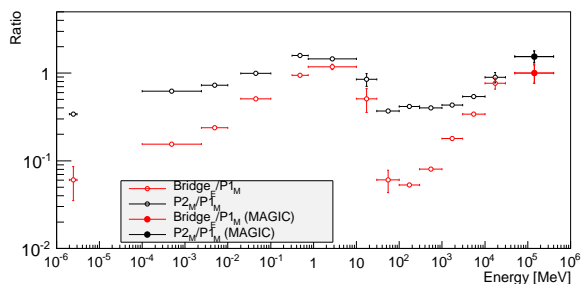


Fig. 3. $P2_M/P1_M$ ratio (black markers) and $Bridge_E/P1_M$ ratio (red markers) as a function of energy. At optical energies (a few eV), the ratios are obtained using the central pixel of the MAGIC camera (Lucarelli et al. 2008). From 100 eV to 100 MeV, ratios are computed based on the light curves shown in Kuiper et al. (2001). From 100 MeV to 30 GeV, *Fermi*-LAT data were used.

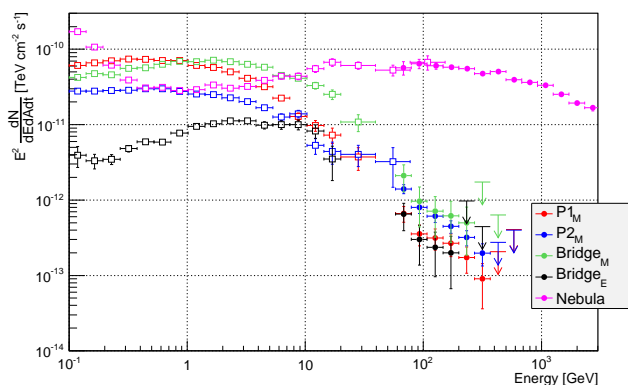


Fig. 4. Spectral energy distributions of the Crab pulsar, $P1_M$, $P2_M$, $Bridge_M$, and $Bridge_E$ measured with *Fermi*-LAT (below 50 GeV) and MAGIC (above 50 GeV). The flux values averaged over the rotation period are plotted.

gion. We estimate the overall systematic uncertainty on the spectral slope to be 0.3.

4. Discussion

In summary, the Crab pulsar above 50 GeV exhibits a light curve with a significant bridge emission between two sharp peaks (Fig. 1). The flux ratios $P2_M/P1_M$ and $Bridge_E/P1_M$ increase with increasing photon energy between 100 MeV and 400 GeV (Figs. 2 and 3). Between 30 GeV and 400 GeV, the fluence in the bridge phase is comparable to that in the P1 phase (Fig. 4). The SEDs in the 50–400 GeV range could be fit with power-law functions for the three phases.

Detection of pulsed VHE emissions favors emission sites in the outer part of the magnetosphere because a strong source attenuation is expected at lower altitudes at these energies. The outer-gap (OG) and the slot-gap models are the most probable explanation of these pulsed γ -rays (Harding et al. 2008; Watters & Romani 2011; Venter et al. 2012). Using an ad hoc extension of the two dimensional meridional OG model to three dimension, Tang et al. (2008) and Takata et al. (2008) reproduced the bridge emission. However, a fully three-dimensional electro-dynamical structure is required to model the phase resolved SEDs (Hiro-tani 2011, 2013).

Alternatively, if a very strong magnetic-field-aligned electric field arises near the light cylinder (LC), pulsed VHE pho-

tons might be also emitted there (Bednarek 2012). Emission from beyond the LC can also explain the double-peaked light curves. Arka & Dubus (2013) demonstrated that a sufficient luminosity and a hard spectrum extending to 100 GeV can be obtained for P1 and P2 via the synchrotron emission by a hot plasma from the current sheet slightly outside the LC, but in this scenario the bridge emission should disappear above 10 GeV. Chkheidze et al. (2013) proposed that synchrotron radiation generated near the LC during the quasi-linear stage of the cyclotron instability can produce the phase-aligned pulsation between radio and γ -rays. However, the formation of a bridge component is not explained in this model.

Although synchrotron luminosity declines sharply beyond the LC, the inverse-Compton process may still be effective there. Aharonian et al. (2012) demonstrated that the observed pulsed flux of the Crab pulsar between 70 GeV and 400 GeV can be explained by up-scattered photons by a particle-dominated wind whose Lorentz factors exceed 5×10^5 at 20–50 LC radii. Although a phase-resolved spectrum is not provided in their paper, the observed $P2/P1$ ratio in VHE could be reproduced if one considers an anisotropic wind. The bridge emission is also predicted, but a special density profile is required to explain

Table 1. Spectral Parameters

phase	F_1^a [$10^{-11}\text{MeV}^{-1}\text{cm}^{-2}\text{s}^{-1}$]	Γ_1^a	E_c^a [GeV]	F_{100}^b [$10^{-11}\text{TeV}^{-1}\text{cm}^{-2}\text{s}^{-1}$]	Γ_2^b
P1 _M	8.87 ± 0.14	1.88 ± 0.01	3.74 ± 0.15	4.18 ± 0.59	3.25 ± 0.39
P2 _M	3.14 ± 0.07	1.97 ± 0.01	7.24 ± 0.64	8.48 ± 0.62	3.27 ± 0.23
Bridge _M	7.70 ± 0.11	1.74 ± 0.01	7.19 ± 0.39	12.2 ± 3.3	3.35 ± 0.79
Bridge _E	0.95 ± 0.04	1.44 ± 0.04	6.94 ± 0.90	3.7 ± 1.1	3.51 ± 0.97

^(a) Spectral parameters obtained by fitting a function $F(E) = F_1(E/1\text{GeV})^{-\Gamma_1} \exp(E/E_c)$ to *Fermi*-LAT data between 100 MeV and 300 GeV

^(b) Spectral parameters obtained by fitting a function $F(E) = F_{100}(E/100\text{GeV})^{-\Gamma_2}$ to MAGIC data between 50 GeV and 400 GeV

Lucarelli, F., Barrio, J. A., Antoranz, P., et al. 2008, Nuclear Instruments and Methods in Physics Research A, 589, 415
 Lyne, A. G., Pritchard, R. S., & Graham-Smith, F. 1993, MNRAS, 265, 1003
 Moralejo, A., Gaug, M., Carmona, E., et al. 2009, ArXiv e-prints
 Muslimov, A. G. & Harding, A. K. 2004, ApJ, 606, 1143
 Nolan, P. L., Abdo, A. A., Ackermann, M., et al. 2012, ApJS, 199, 31
 Nolan, P. L., Arzoumanian, Z., Bertsch, D. L., et al. 1993, ApJ, 409, 697
 Takata, J., Chang, H.-K., & Shibata, S. 2008, MNRAS, 386, 748
 Takata, J., Shibata, S., Hirofani, K., & Chang, H.-K. 2006, MNRAS, 366, 1310
 Tang, A. P. S., Takata, J., Jia, J. J., & Cheng, K. S. 2008, ApJ, 676, 562
 Venter, C., Johnson, T. J., & Harding, A. K. 2012, ApJ, 744, 34
 Watters, K. P. & Romani, R. W. 2011, ApJ, 727, 123

- ¹ IFAE, Campus UAB, E-08193 Bellaterra, Spain
- ² Università di Udine, and INFN Trieste, I-33100 Udine, Italy
- ³ INAF National Institute for Astrophysics, I-00136 Rome, Italy
- ⁴ Università di Siena, and INFN Pisa, I-53100 Siena, Italy
- ⁵ Croatian MAGIC Consortium, Rudjer Boskovic Institute, University of Rijeka and University of Split, HR-10000 Zagreb, Croatia
- ⁶ Max-Planck-Institut für Physik, D-80805 München, Germany
- ⁷ Universidad Complutense, E-28040 Madrid, Spain
- ⁸ Inst. de Astrofísica de Canarias, E-38200 La Laguna, Tenerife, Spain
- ⁹ University of Łódź, PL-90236 Lodz, Poland
- ¹⁰ Deutsches Elektronen-Synchrotron (DESY), D-15738 Zeuthen, Germany
- ¹¹ ETH Zurich, CH-8093 Zurich, Switzerland
- ¹² Universität Würzburg, D-97074 Würzburg, Germany
- ¹³ Centro de Investigaciones Energéticas, Medioambientales y Tecnológicas, E-28040 Madrid, Spain
- ¹⁴ Technische Universität Dortmund, D-44221 Dortmund, Germany
- ¹⁵ Università di Padova and INFN, I-35131 Padova, Italy
- ¹⁶ Università dell'Insubria and INFN Milano Bicocca, Como, I-22100 Como, Italy
- ¹⁷ Unitat de Física de les Radiacions, Departament de Física, and CERES-IEEC, Universitat Autònoma de Barcelona, E-08193 Bellaterra, Spain
- ¹⁸ Institut de Ciències de l'Espai (IEEC-CSIC), E-08193 Bellaterra, Spain
- ¹⁹ Japanese MAGIC Consortium, Division of Physics and Astronomy, Kyoto University, Japan
- ²⁰ Academia Sinica, Institute of Astronomy and Astrophysics (ASIAA), P.O. Box: 23-141, Taipei, Taiwan
- ²¹ Finnish MAGIC Consortium, Tuorla Observatory, University of Turku and Department of Physics, University of Oulu, Finland
- ²² Inst. for Nucl. Research and Nucl. Energy, BG-1784 Sofia, Bulgaria
- ²³ Universitat de Barcelona, ICC, IEEC-UB, E-08028 Barcelona, Spain
- ²⁴ Università di Pisa, and INFN Pisa, I-56126 Pisa, Italy
- ²⁵ ICREA and Institut de Ciències de l'Espai (IEEC-CSIC), E-08193 Bellaterra, Spain
- ²⁶ now at: NASA Goddard Space Flight Center, Greenbelt, MD 20771, USA and Department of Physics and Department of Astronomy, University of Maryland, College Park, MD 20742, USA
- ²⁷ now at Ecole polytechnique fédérale de Lausanne (EPFL), Lausanne, Switzerland
- ²⁸ now at Finnish Centre for Astronomy with ESO (FINCA), Turku, Finland
- ²⁹ also at INAF-Trieste
- ³⁰ now at Stockholm University, Oskar Klein Centre for Cosmoparticle Physics, SE-106 91 Stockholm, Sweden